Manuscript

Available online at www.sciencedirect.com

ScienceDirect

Graphical Models 00 (2021) 1–13

Graphical Models

Heterogeneous Porous Scaffold Generation Using Trivariate B-spline Solids and Triply Periodic Minimal Surfaces

CVM Paper 51

Abstract

A porous scaffold is a three-dimensional network structure composed of a large number of pores, and triply periodic minimal surfaces (TPMSs) are one of the conventional tools for designing porous scaffolds. However, discontinuity, incompleteness, and high storage space requirements are the three main shortcomings of porous scaffold design using TPMSs. In this study, we developed an effective method for heterogeneous porous scaffold generation to overcome the abovementioned shortcomings of porous scaffold design. The input of the proposed method is a trivariate B-spline solid with a cubic parametric domain. The proposed method first constructs a threshold distribution field (TDF) in the cubic parametric domain, and then produces a continuous and complete TPMS within it. Finally, by mapping the TPMS in the parametric domain to the trivariate B-spline solid, a continuous and complete porous scaffold is generated. Moreover, we defined a new storage space-saving file format based on the TDF to store porous scaffolds. The experimental results presented in this paper demonstrate the effectiveness and efficiency of the method using a trivariate B-spline solid, as well as the superior space-saving of the proposed storage format.

Keywords: Porous scaffold, Trivariate B-spline solids, Triply periodic minimal surfaces, Parametric domain

1. Introduction

Porous structures are widely found in natural objects, such as trabecular bones, wood, and cork, which have many appealing properties, such as low weight and large internal surface area. Recently, triply periodic minimal surfaces (TPMSs) have been widely employed in the design of porous scaffolds [1]. A TPMS is a type of minimal surface with periodicity in three independent directions of the three-dimensional Euclidean space, and is represented by an implicit equation [2]. Generally speaking, porous scaffold design methods based on TPMS can be classified into two categories. In the first class of methods, a volume mesh model is embedded in an ambient TPMS, and the intersection of them is taken as the porous scaffold by Boolean operations or marching tetrahedra algorithm [3, 4, 5, 6]. In the second class of methods, a regular TPMS unit, i.e., the TPMS in a whole period, is transformed into each hexahedron of a hexahedron mesh model, thus generating a porous scaffold [7, 8, 9]. However, the first class of methods can generate incomplete TPMS units near the boundary of a volume mesh model, leading to poor mechanical performance. The second class of methods may cause discontinuities between two adjacent TPMS units, and, more seriously, the porosity is difficult to control.

The continuity and completeness are two key ingredients to a porous scaffold. On the one hand, continuities in the scaffolds can positively influence the fluid flow between the two adjacent regions, which will in turn be beneficial to cell penetration, and transport of nutrients and growth factors in and out of the scaffolds [10]. On the other hand, the completeness of the scaffolds' component is related to the mechanical performance of the scaffold. In addition, the scaffolds generated by TPMS-based methods can provide a larger surface for cell attachment, so that the scaffolds degrade faster and the tissues grow faster than that of traditional methods, due to the high specific surface area of TPMS [11, 12].

More seriously, due to the complicated geometric and topological structure of the porous scaffold, its storage cost is very large, usually requiring hundreds of megabytes (MB) [8]. The large storage cost becomes the bottleneck in porous scaffold generation and processing.

In this study, we developed a method for generating heterogenous porous scaffolds in a trivariate B-spline solid with TPMS designed in the parametric domain. Specifically, given a trivariate B-spline solid, a threshold distribution field (TDF) is first constructed in the cubic parametric domain, as well as a TPMS. By mapping the TPMS in the parametric domain to the B-spline solid, a porous scaffold is produced. All of the TPMS units generated in the porous scaffold are complete, and adjacent TPMS units are continuously stitched. Moreover, based on the TDF in the parametric domain, a new porous scaffold storage format is designed for saving storage space. To summarize,

the main contributions of this study are as follows:

- A trivariate B-spline solid is employed to generate porous scaffolds, which ensures completeness of TPMS units, and continuity between adjacent TPMS units.
- Porous scaffolds are easy to design and modify using the TDF defined in the parametric domain of the B-spline solid.
- A storage format for porous scaffolds is developed, which saves significant storage space.

The remainder of this paper is organized as follows. In Section 1.1, we review related work on the porous scaffold design and B-spline solid generation. In Section 2, preliminaries on trivariate B-spline solid and TPMS are introduced. Then, the heterogeneous porous scaffold generation method using a trivariate B-spline solid and TPMS is presented in detail in Section 3. In Section 4, some experimental examples are presented to demonstrate the effectiveness of the developed method. Finally, Section 5 concludes the paper.

1.1. Related work

In this section, we review some related work on porous scaffold design and trivariate B-spline solid generation methods.

Porous scaffold design: In recent years, TPMS has been of special interest to the porous scaffold design community owing to its excellent properties, and many scaffold design methods have been developed based on TPMS. Rajagopalan and Robb [13] made the first attempt to design tissue scaffolds based on Schwarz's primitive minimal surface, which is a type of TPMS. Moreover, the other two typical TPMSs (Schwarz's diamond surface and Schoen's gyroid surface) are constructed by employing K3DSurf software to design tissue scaffolds [14], which achieve a gradient change of gyroid structure in terms of pore size by adding a linear equation into the TPMS function.

To reduce the time consumed in the trimming and re-meshing process of Boolean operations, a tissue scaffold design method based on a hybrid method of distance field and TPMS was proposed in [3]. Moreover, to make the porosity easier to control in designing a heterogeneous porous scaffold, Yoo [4] introduced a method based on an implicit interpolation algorithm that uses the thin-plate radial basis function. Similar to the method of Yoo [4], Yang et al. [5] introduced the sigmoid function and Gaussian radial basis function to design tissue scaffolds. However, the hexahedral mesh-based porous scaffold generation methods cannot ensure continuity between adjacent TPMS units.

Recently, in consideration of the increasing attention towards gradient porous scaffolds, Shi et al. [9] utilized the TPMS and sigmoid function to generate functional gradient bionic porous scaffolds from Micro-CT data reconstruction. Feng et al. [6] proposed a method to design porous scaffold based on T-spline solids and TPMS, and analyzed the parameter influences on the ratio of volume to surface area and porosity. Subsequently, Li et al. [15, 16] adopted trivariate T-splines in modeling and slicing heterogeneous porous structures. In addition, a heterogeneous methodology for modeling porous scaffolds using a parameterized hexahedral mesh and TPMS was developed by Chen et al. [8].

Trivariate B-spline solid generation: Trivariate B-spline solid modeling methods are developed mainly for producing three dimensional physical domain in isogeometric analysis [17]. Specifically, to analyze arterial blood flow through isogeometric analysis, Zhang et al. [18] introduced a skeleton-based method of generating trivariate non-uniform rational basis spline (NURBS) solids. In [19], a tetrahedral mesh model is parameterized through discrete volumetric harmonic functions and a cylinder-like trivariate B-spline solid is generated. Aigner et al. [20] proposed a variational framework for generating NURBS parameterizations of swept volumes using the given boundary conditions and guiding curves. Optimization approaches have been developed for filling boundary-represented models to produce trivariate B-spline solids with positive Jacobian values [21, 22]. Moreover, a discrete volume parameterization method for tetrahedral mesh models and an iterative fitting algorithm have been presented for trivariate B-spline solid generation [23].

2. Preliminaries

2.1. Trivariate B-spline solid

A B-spline curve of order $p+1$ is formed by several piecewise polynomial curves of degree p, and a B-spline curve is $C^{p+1-\mu}$ continuous at its breakpoints with multiplicity μ [24]. A knot vector $U = \{u_0, u_1, \ldots, u_{m+p+1}\}$ is defined by a set of breakpoints $u_0 \le u_1 \le \cdots \le u_{m+p+1}$.

A trivariate B-spline solid of degree (p, q, r) is a tensor product volume defined as

$$\boldsymbol{P}(u,v,w) = \sum_{i=0}^{m}\sum_{j=0}^{n}\sum_{k=0}^{l} N_{i,p}(u)N_{j,q}(v)N_{k,r}(w)\boldsymbol{P}_{ijk}, \tag{1}$$

where $\boldsymbol{P}_{ijk},\ i = 0, 1, \cdots, m,\ j = 0, 1, \cdots, n,\ k = 0, 1, \cdots, l$ are control points in the u, v and w directions, and

$$N_{i,p}(u), N_{j,q}(v), N_{k,r}(w)$$

are the B-spline basis functions of degree p in the u direction, degree q in the v direction, and degree r in the w direction, with parametric domain $[0, 1] \times [0, 1] \times [0, 1]$.

In this study, the input to our porous scaffold generation algorithm is a trivariate B-spline solid (Eq. (1)) that represents geometry at a macro-structural scale. The B-spline solid can be generated either by fitting the mesh vertices of a tetrahedral mesh model [23], or filling a closed triangular mesh model [22].

2.2. Triply periodic minimal surface

TPMS is a competitive alternative for representing the pore-volume structure of tissue engineering scaffolds. Because the four types of TPMS (P, D, G, and I-WP types) possess larger smooth surface area, compared with the other types of TPMS, they are widely employed to design porous scaffolds [13, 14].

The most frequently employed way for describing a TPMS is to approximate the TPMS using a periodic nodal surface defined by a Fourier series [25],

$$\psi(\boldsymbol{r}) = \sum_k A_k cos[2\pi(\boldsymbol{h}_k \cdot \boldsymbol{r})/\lambda_k - P_k] = C, \tag{2}$$

where $\boldsymbol{r}$ is the location vector in the Euclidean space, A_k is the amplitude, $\boldsymbol{h}_k$ is the k^{th} lattice vector in the reciprocal space, λ_k is the wavelength of the period, P_k is the phase shift, and C is the threshold constant. Specifically, a TPMS is the implicit surface defined by $\psi(\boldsymbol{r}) = C$ (Eq. (2)). Please refer to [26] for more details on the abovementioned parameters. The nodal approximations of P, D, G, and I-WP types of TPMSs, which were presented in [2], are listed in Table 1, where the valid range of C guarantees that the implicit surface is complete.

In TPMS-based porous scaffold design methods, the threshold C (Eq. (2)) controls the porosity, and the coefficients ρ_u, ρ_v, and ρ_w (refer to Table 1), called *period coefficients*, affect the period of the TPMS and the pore size. The effects of the two types of parameters in porous scaffold design have been discussed in detail in the literature [6]. Additionally, in this study, the marching tetrahedra (MT) algorithm [27] is employed to extract the TPMS (Fig. 1).

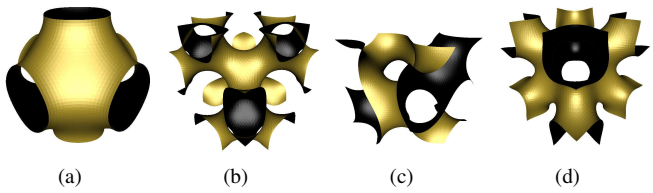

(a) (b) (c) (d)

Figure 1. Four types of TPMS units. (a) P-type. (b) D-type. (c) G-type. (d) I-WP-type.

Moreover, we define three types of *volume TPMS structures* (refer to Eq. (2)):

- *pore structure* represented by $\psi \geq C$,
- *rod structure* represented by $\psi \leq C$,
- *sheet structure* represented by $C - \epsilon \leq \psi \leq C$,

where ϵ is set to 0.2 in our implementation. However, the triangular meshes of the three types of volume TPMS structures, generated by the polygonization, are open on the six boundary faces of the parameter domain, so they should be closed to form a solid. Take the pore structure ($\psi \geq C$) as an example. In the polygonization procedure of the TPMS $\psi = C$ by the MT algorithm, the triangles on the boundary faces of the parameter domain are categorized into two classes by the iso-value curve $\psi = C$ on the boundary faces: outside triangles, where the values of ψ at the vertices of these triangles are larger than or equal to C, and inside triangles, where the values of ψ at the vertices of these triangles are smaller than or equal to C. Therefore, the pore structure can be closed by adding the outside triangles into the triangular mesh generated by polygonizing $\psi = C$.

As stated above, the method developed in this paper can ensure completeness of TPMS units, and continuity between adjacent TPMS units. On the one hand, completeness means that each TPMS unit in the generated porous scaffold is complete. On the other hand, unless otherwise specified, continuity in this paper refers to C^0 continuity between adjacent surfaces.

Algorithm 1 Heterogeneous porous scaffold generation

Input: TPMS type, structure type, period coefficients (ρ_u, ρ_v, ρ_w), trivariate B-spline solid, porosity requirements.
Output: Heterogeneous porous scaffold.
1: Construction of the initial TDF;
2: Calculation of the porosity in the physical domain;
3: **while** not meeting the porosity requirements **do**
4: Porosity adjustment in the TDF;
5: Calculation of the porosity in the physical domain;
6: **end while**
7: Generation of the volume TPMS structure;
8: Generation of the heterogeneous porous scaffold.

3. Methodology of Porous Scaffold Design

The whole algorithm of the developed heterogeneous porous scaffold generation method is illustrated in Algorithm 1. Specifically, given a trivariate B-spline solid as the *physical domain*, we design a method for constructing the TDF in its cubic parametric domain. In order to ensure the generated porous scaffold meets the engineering requirements, the TDF is modified iteratively until the requirements are satisfied. Based on the TDF, a *volume TPMS structure* is generated in the parmetric domain. Moreover, by mapping the volume TPMS structure in the parametric domain to the physical domain through the B-spline solid function (Eq. (1)), a porous scaffold with completeness and continuity is produced. The details of the porous scaffold design method are elucidated in the following sections.

3.1. Threshold distribution field (TDF) construction

To design heterogeneous porous scaffolds, we alter the threshold C to a trivariate B-spline function $C(u, v, w)$ defined on the parametric domain of a trivariate B-spline solid, which is called *threshold distribution field* (TDF). Then, the *TPMS in the parametric domain* is represented by the zero-level surface of,

$$f(u, v, w) = \psi(u, v, w) - C(u, v, w) = 0. \tag{3}$$

Therefore, the TDF plays a critical role in the heterogeneous porous scaffold generation, and how to design the TDF becomes a key problem in the porous scaffold design.

Because the TDF is represented as a trivariate B-spline function $C(u, v, w)$, it facilitates the design of TDF, as well as the porous scaffold. In the following, we presented a methodology framework for designing a TDF. Users can develop their own method to generate a TDF based on the methodology framework. Specifically, the parametric domain of a trivariate B-spline solid is first discretized into a dense grid (in our implementation, it is discretized into a grid with a resolution of

Table 1. Nodal approximations of typical TPMS units.

TPMS	Nodal approximations	Valid range of C
Schwarz's P Surface	$\psi_P(u,v,w) = cos(\rho_u u) + cos(\rho_v v) + cos(\rho_w w) = C$	$[-0.8, 0.8]$
Schwarz's D Surface	$\psi_D(u,v,w) = cos(\rho_u u)cos(\rho_v v)cos(\rho_w w) - sin(\rho_u u)sin(\rho_v v)sin(\rho_w w) = C$	$[-0.6, 0.6]$
Schoen's G Surface	$\psi_G(u,v,w) = sin(\rho_u u)cos(\rho_v v) + sin(\rho_v v)cos(\rho_w w) + sin(\rho_w w)cos(\rho_u u) = C$	$[-0.8, 0.8]$
Schoen's I-WP Surface	$\psi_{I-WP}(u,v,w) = 2[cos(\rho_u u)cos(\rho_v v) + cos(\rho_v v)cos(\rho_w w) + cos(\rho_w w)cos(\rho_u u)]$ $-[cos(2\rho_u u) + cos(2\rho_v v) + cos(2\rho_w w)] = C$	$[-2.0, 2.0]$

$50 \times 50 \times 50$), called a *parametric grid*. Then, the threshold values at the grid vertices are assigned (for example, using the techniques presented later in this section), constituting a *discrete TDF*. Finally, the discrete TDF is fitted by a trivariate B-spline function, which is taken as the TDF $C(u,v,w)$, i.e.,

$$C(u,v,w) = \sum_{i=0}^{n_u}\sum_{j=0}^{n_v}\sum_{k=0}^{n_w} N_{i,p}(u)N_{j,q}(v)N_{k,r}(w)C_{ijk}, \qquad (4)$$

where the scales C_{ijk} are the control points of the trivariate B-spline function.

Next, we present two techniques for generating the discrete TDF, i.e., physical domain based technique and parametric domain based technique, by which a threshold value $C_{\alpha,\beta,\gamma}$ is assigned to the parametric grid vertex with index (α,β,γ). However, users can develop their methods for discrete TDF generation to satisfy specific requirements.

Physical domain based technique. Initially, the parametric grid is mapped into the B-spline solid (i.e., the physical domain) to generate a grid, called *physical grid*, and all of the scalar values at the physical grid vertices are set to 0. Then, some physical quantities (here, we take the porosity values as an example) can be specified at the boundary physical grid vertices. Next, the porosities at the boundary grid vertices are diffused into the inner physical grid vertices by the Laplace smoothing operation [28], and then the entire physical grid is filled. Furthermore, the porosities defined at the physical grid vertices are mapped back to the parametric grid. After changing the porosities to the threshold values by the relationship between them (refer to Appendix B and Figs. 4(a)-4(b)), and transforming them into the valid threshold range (Table 1) according to the type of TPMS being produced, they are taken as the threshold values $C_{\alpha,\beta,\gamma}$ at the parametric grid vertices. In this way, the discrete TDF is constructed based on the porosities defined at the boundary physical grid vertices. In Fig. 2, the mean curvatures of the boundary surface is taken as the porosities (Fig. 2(a)), and then the discrete TDF is generated based on the mean curvatures (Fig. 2(b)).

Parametric domain based technique. The threshold values $C_{\alpha,\beta,\gamma}$ in the parametric grid vertex with index (α,β,γ) can be directly assigned by a function prescribed by users. For example, we define two types of distribution functions, including radial distribution (Eq. (5)) and axial distribution (Eq. (6)),

$$C_{\alpha,\beta,\gamma} = 1.4 * max\{|\alpha - 0.5|, |\beta - 0.5|\} - 0.6, \qquad (5)$$

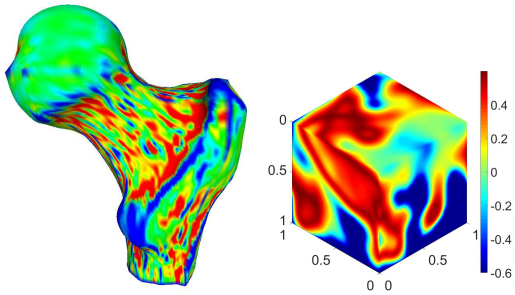

(a) (b)

Figure 2. Physical domain based technique. (a) Mean curvatures on the boundary surface of a trivariate B-spline solid. (b) Discrete TDF based on the mean curvatures.

$$C_{\alpha,\beta,\gamma} = 1.2 * (\gamma - 0.5), \qquad (6)$$

which are illustrated in Figs. 3(a) and 6(b), respectively. Note that the values $C_{\alpha,\beta,\gamma}$ should be linearly transformed into the valid threshold range (Table 1) according to the type of volume TPMS structure being produced.

TDF generation by data fitting. After the discrete TDF is generated, it is fitted with a trivariate B-spline function (Eq. (4)), using the least squares progressive-iteration approximation (LSPIA) method [29]. The indices of the grid vertices, i.e., (α,β,γ), are the natural parametrization of the vertices. For the purpose of B-spline fitting, they are normalized into the interval $[0,1] \times [0,1] \times [0,1]$, denoted as $(u_\alpha, v_\beta, w_\gamma)$. The knot vectors of the B-spline function (Eq. (4)) are uniformly defined under the Bézier end condition. In our implementation, the size of the control grid of the trivariate B-spline function is taken as $20 \times 20 \times 20$, and the initial values of the control points of the B-spline function (Eq. (4)) are produced by linear interpolation of the discrete TDF.

Suppose the LSPIA iteration has been performed for l steps, and the l^{th} B-spline function $C^{(l)}(u,v,w)$ is constructed as:

$$C^{(l)}(u,v,w) = \sum_{i=0}^{n_u}\sum_{j=0}^{n_v}\sum_{k=0}^{n_w} N_{i,p}(u)N_{j,q}(v)N_{k,r}(w)C^{(l)}_{ijk}. \qquad (7)$$

To generate the $(l+1)^{th}$ B-spline function $C^{(l+1)}(u,v,w)$, the *difference vector for each parametric grid vertex* is calculated,

$$\delta^{(l)}_{\alpha,\beta,\gamma} = C_{\alpha,\beta,\gamma} - C^{(l)}(u_\alpha, v_\beta, w_\gamma), \qquad (8)$$

where $C_{\alpha,\beta,\gamma}$ is the threshold value at the vertex (α,β,γ), and $(u_\alpha, v_\beta, w_\gamma)$ are its parameters. Each difference vector $\delta^{(l)}_{\alpha,\beta,\gamma}$ is distributed to the control points $C^{(k)}_{i,j,k}$ if the corresponding basis functions $N_{i,p}(u_\alpha)N_{j,q}(v_\beta)N_{k,r}(w_\gamma)$ are non-zero. Moreover, a weighted average of all difference vectors distributed to a control point is taken, leading to the *difference vector for the control point*,

$$\Delta^{(l)}_{ijk} = \frac{\sum_{(\alpha,\beta,\gamma)\in I_{ijk}} N_{i,p}(u_\alpha)N_{j,q}(v_\beta)N_{k,r}(w_\gamma)\delta^{(l)}_{\alpha,\beta,\gamma}}{\sum_{(\alpha,\beta,\gamma)\in I_{ijk}} N_{i,p}(u_\alpha)N_{j,q}(v_\beta)N_{k,r}(w_\gamma)}, \tag{9}$$

where I_{ijk} is the set of indices (α,β,γ) such that

$$N_{i,p}(u_\alpha)N_{j,q}(v_\beta)N_{k,r}(w_\gamma) \neq 0.$$

Next, the $(l+1)^{th}$ control points $C^{(l+1)}_{ijk}$ are formed by adding the difference vectors $\Delta^{(l)}_{ijk}$ to the l^{th} control points,

$$C^{(l+1)}_{ijk} = C^{(l)}_{ijk} + \Delta^{(l)}_{ijk}. \tag{10}$$

Thus, the $(l+1)^{th}$ B-spline function $C^{(l+1)}(u,v,w)$ is produced:

$$C^{(l+1)}(u,v,w) = \sum_{i=0}^{n_u}\sum_{j=0}^{n_v}\sum_{k=0}^{n_w} N_{i,p}(u)N_{j,q}(v)N_{k,r}(w)C^{(l+1)}_{ijk}. \tag{11}$$

The computational complexity for the iteration is $O(\mathcal{MN})$, where $\mathcal{M}$ is the number of control points $C^{(l)}_{ijk}$, and $\mathcal{N}$) is the number of data points $C_{\alpha\beta\gamma}$. The convergence and the stability of LSPIA iteration have been discussed in detail in Ref.[29]. After the iterations stop, the result is taken as the TDF $C(u,v,w)$ in the parametric domain.

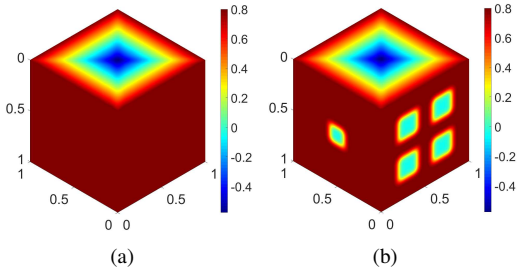

Figure 3. Local modification on TDF. (a) TDF generated based on the prescribed function (5). (b) TDF after local modification.

3.2. Local modification

With the TDF $C(u,v,w)$, the TPMS (Eq. (3)) in the parametric domain can be generated. By mapping the TPMS into the trivariate B-spline solid, a porous scaffold is produced. However, if the generated porous scaffold does not satisfy the practical engineering requirements, the TDF $C(u,v,w)$ can be locally modified in the parametric domain, and then the porous scaffold can be rebuilt to meet the practical requirements (refer to Section 3.3).

To locally modify the TDF, some vertices of the parametric grid are first chosen, and the threshold values there are changed to the desired values. Then, a *local* LSPIA iteration is invoked to fit the changed values at the chosen vertices. In the local LSPIA iteration, the difference vector δ (Eq. (8)) is calculated only at the chosen vertices, and we adjust only the control points to which the difference vectors δ are distributed. The other control points remain unchanged. As illustrated in Fig. 3, the TDF in Fig. 3(b) is generated by locally modifying the TDF in Fig. 3(a) using the method presented above.

3.3. Porosity preservation

The porosity is an important parameter in porous scaffold design, which directly influences the transport of nutrition and waste. The porosity of porous scaffolds designed by TPMS units can be controlled by adjusting the threshold C (Table 1). The relationship between the porosity and the threshold C is illustrated in Figs.4(a)-4(c), and the mathematical functions between the porosity and C are presented in Appendix B. It should mention that, for the sheet structure (Fig. 4(c)), the porosity is insensitive to the change of threshold C. When the threshold C varies in its valid range, the porosity changes very small (Fig. 4(c)).

In practice, the porous scaffold is usually required to reach predefined porosity values Por_ℓ at some physical grid vertices (x_ℓ, y_ℓ, z_ℓ), with parameters (u_ℓ, v_ℓ, w_ℓ), $\ell = 0, 1, \cdots, \mathcal{N}-1$. In order to make the generated porous scaffold meet the porosity requirements, a constrained optimization problem is formulated (Eq. (12)), where the optimization variables are the control points of the TDF, arranged in the lexicographical order, i.e.,$(C_{000}, C_{001}, \cdots, C_{n_u,n_v,n_w})$.

$$\begin{aligned} &\min E = \sum_{\ell=0}^{\mathcal{N}-1} \left\| Por(C_{000}, C_{001}, \cdots, C_{n_u,n_v,n_w}; u_\ell, v_\ell, w_\ell) - Por_\ell \right\|^2 \\ &s.t.\ C_{000}, C_{001}, \cdots, C_{n_u,n_v,n_w} \text{ are in the valid range,} \end{aligned} \tag{12}$$

where $Por(C_{000}, C_{001}, \cdots, C_{n_u,n_v,n_w}; u_\ell, v_\ell, w_\ell)$ is the porosity value of the porous scaffold at the parameter (u_ℓ, v_ℓ, w_ℓ).

We employ the gradient descent method to solve the minimization problem (Eq. (12)). The gradient vector of the objective function is,

$$\nabla E = \left(\frac{\partial E}{\partial C_{000}}, \cdots, \frac{\partial E}{\partial C_{ijk}}, \cdots, \frac{\partial E}{\partial C_{n_u,n_v,n_w}} \right). \tag{13}$$

In the optimization, the control points C_{ijk} move along the gradient vectors to produce the new control points, i.e.,

$$C^{new}_{ijk} = C_{ijk} + \tau \frac{\partial E}{\partial C_{ijk}},$$

where $\tau \in (0,1]$ is a weight. In our implementation, we discretize $\tau \in (0,1]$ to $\{\frac{1}{n}, \frac{2}{n}, \cdots, \frac{n}{n}\}$ with $n = 20$, and select a weight as large as possible to minimize the objective function (12).

Because the relationship between the variables

$$C_{000}, C_{001}, \cdots, C_{n_u,n_v,n_w}$$

and the objective function E is complicated, the expressions of the partial derivatives in the gradient vector (Eq. (13)) are

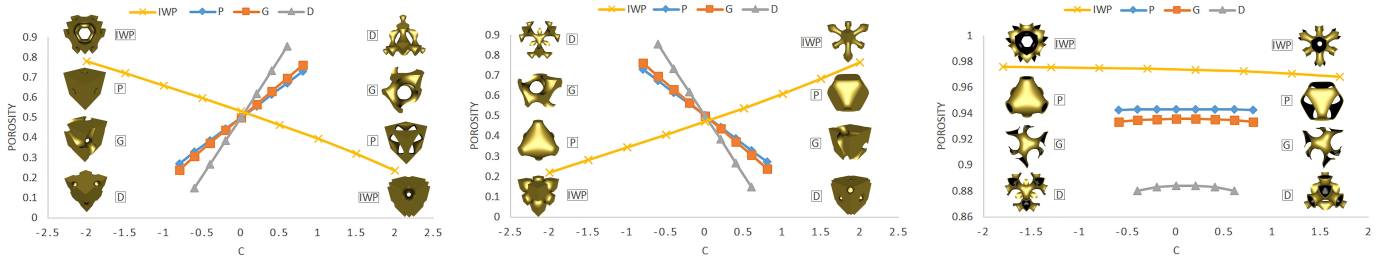

(a) (b) (c)

Figure 4. Relationship between the threshold C and the porosity of the four types of TPMSs based on pore structures (a), rod structures (b), and sheet structures (c), respectively.

hard to be deduced. Therefore, in calculating the gradient vector (Eq. (13)), we replace the partial derivatives with the finite differences,

$$\frac{\partial E}{\partial C_{ijk}} \approx \frac{E(\cdots, C_{ijk}+\delta, \cdots) - E(\cdots, C_{ijk}, \cdots)}{\delta},$$

where $i = 0, 1, \cdots, n_u$, $j = 0, 1, \cdots, n_v$, $k = 0, 1, \cdots, n_w$, and δ is a tiny increment, taken as 0.02 in our implementation.

The initial TDF is constructed as follows. Firstly, the threshold values C_ℓ corresponding to the predefined porosity values Por_ℓ can be calculated using the relationship between the porosity and the threshold C, as presented in Figs. 4(a)-4(b) and Appendix B. Secondly, the threshold values at the corresponding parametric grid vertices (u_ℓ, v_ℓ, w_ℓ) are set as $C_\ell, \ell = 0, 1, \cdots, \mathcal{N}-1$. Finally, the initial TDF $C(u, v, w)$ in the parametric domain is generated by fitting the threshold values at parametric grid vertices using LSPIA. The error of the porosity in the physical domain is defined as,

$$err = \frac{E}{\mathcal{N}}, \tag{14}$$

In our implementation, the terminate condition is defined as,

$$\left|\frac{err_i - err_{i-1}}{err_0}\right| < 10^{-4}, \quad i \geq 1, \tag{15}$$

where err_i denotes the error of the porosity after the i-th iteration, and err_0 denotes the initial error. And for each iteration, the computational complexity is $O(\mathcal{M}^2\mathcal{N})$, where $\mathcal{M}$ is the number of the control points. The convergence and the stability of the gradient descent method has been discussed in detail in several references, such as Ref.[30].

In our experiments, the gradient descent method converges rapidly. For example (Fig. 5), a uniform porosity of 0.5 is predefined at all physical grid vertices. Fig. 5(a) is the porous scaffold generated with the initial TDF. Fig. 5(b) is the heterogeneous porous scaffold after optimization, where the uniformity of the porosity is improved. As we can see, the pore size in the red circles changes obviously. As shown in Fig. 5(c), the error is reduced from 0.0111 to 0.0012 after 2 iterations, and the iteration is terminated at the 27-th step.

It should be pointed out that, the porosity preservation method cannot be applied in the design of sheet structures, because the porosity of a sheet structure is nearly constant as a function of the threshold C (Fig. 4(c)). In other words, for the sheet structures, the porosity can vary just in a vary small range.

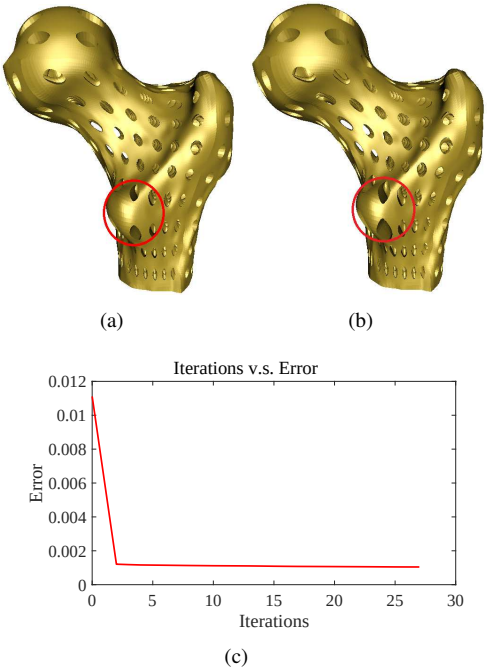

(a) (b) (c)

Figure 5. Porosity preservation: the predefined porosities at all physical grid vertices are 0.5. (a) Porous scaffold before optimization. (b) Porous scaffold after optimization. (c) Plot of error v.s. iterations.

Porosity Calculation: The porosity Por of the heterogeneous porous scaffold at the point (x, y, z) in the physical domain with the parameter (u, v, w) can be calculated by the following formula,

$$Por = \frac{\int_{\Omega_{void}} Jac(u, v, w) d\Omega}{\int_{\Omega} Jac(u, v, w) d\Omega},$$

where Ω is a cuboid region centered at the point (u, v, w) in the parametric domain, with size $\frac{1}{\rho_u} \times \frac{1}{\rho_v} \times \frac{1}{\rho_w}$ (equal to the size of a TPMS unit in the parametric domain), Ω_{void} is the pore region in Ω, and $Jac(u, v, w)$ is the Jacobian value of the B-

spline solid mapping (Eq. (1)) at (u, v, w). In our implementation, the porosities *Por* is calculated using the Gaussian quadrature rule [30]. Note that, the calculation of the porosity *Por* of heterogeneous porous scaffold in the physical domain is performed in the parametric domain, owing to the Jacobian value $Jac(u, v, w)$ of the B-spline solid mapping(Eq. (1)). Therefore, the heterogeneous porous scaffold in the physical domain is not required to be generated for the calculation of its porosity.

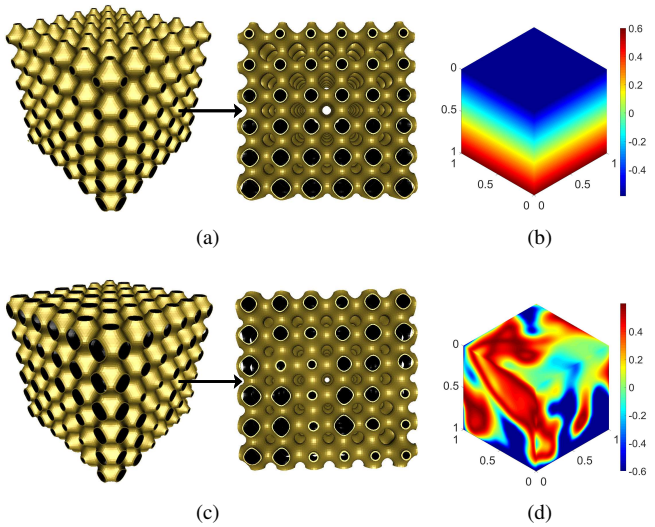

Figure 6. Generation of the TPMSs (with perspective-view and side-view drawing) (a,c) based on the corresponding TDF in the parametric domain (b,d). Note that the porosity of the TPMS is controlled by the TDF.

3.4. Generation of heterogeneous porous scaffold

Till now, there is only one unknown in the heterogeneous porous scaffold generation: the period coefficients ρ_u, ρ_v, ρ_w (Table 1). It is worth noting that the internal connectivity of the scaffold is crucial to the transferring performance of the scaffold. The period coefficients ρ_u, ρ_v, ρ_w (Table 1) can be employed to adjust the number of TPMS units, as well as the size of TPMS units in the three parametric directions. The values of the period coefficients ρ_u, ρ_v, ρ_w used in the examples in this paper are listed in Table 2.

After the TDF and the period coefficients are both determined, the TPMS in the parametric domain (Eq. (3)), i.e.,

$$f(u, v, w) = \psi(u, v, w) - C(u, v, w) = 0,$$

can be determined and polygonized into a triangular mesh. For this purpose, the cubic parametric domain is uniformly divided into a grid. In our implementation, to balance the accuracy and storage cost of the porous scaffold, the parametric domain is divided into a $100 \times 100 \times 100$ grid. Moreover, the volume TPMS structures can also be generated, just as presented in Section 2.2. In Figs. 6(a) and 6(c), we illustrate the TPMSs (sheet structure) calculated based on the TDFs in Figs. 6(b) and 6(d).

Finally, the heterogeneous porous scaffold in the trivariate B-spline solid can be generated by mapping the volume TPMS structures into the trivariate B-spline solid. Because the TPMS in the parametric domain is a unitary surface and the trivariate B-spline solid mapping (Eq. (1)) is C^2 continuity, each TPMS unit is complete, and adjacent TPMS units are continuous along their boundary. Therefore, the heterogeneous porous scaffold in the trivariate B-spline solid is ensured to be complete and continuous.

3.5. Storage format

Owing to their complicated geometric and topological structure, the storage costs for porous scaffolds are very large, usually requiring hundreds of megabytes (MB) (refer to Table 2). Therefore, the large storage cost becomes the bottleneck in porous scaffold generation and processing. In this study, we developed a new porous scaffold storage format that reduces the storage cost of porous scaffolds significantly. Using the new storage format, the space required to store the porous scaffold models presented in this paper ranges from 0.538 MB to 0.947 MB, while the storage space using the traditional STL file format ranges from 407.188 MB to 1359.087 MB. Thus, the new storage format reduces the storage requirement by at least 99% compared with the traditional STL file format. Moreover, the generation of heterogeneous porous scaffolds from the new file format costs just a few seconds (Table 2).

Specifically, because the TDF in the parametric domain and the period coefficients(Table 1) entirely determine the heterogeneous porous scaffold in a trivariate B-spline solid, the new storage format is required to store only the following information:

- TPMS type,
- structure type,
- period coefficients ρ_u, ρ_v, ρ_w,
- control points of the TDF $C(u, v, w)$,
- knot vectors of the TDF $C(u, v, w)$,
- control points of the B-spline solid $P(u, v, w)$,
- knot vectors of the B-spline solid $P(u, v, w)$.

Therefore, the new storage format is called the *TDF format*, and is summarized in Appendix A for clarity.

4. Implementation, Results and Discussions

The developed heterogeneous porous scaffold generation method is implemented with the C++ programming language and tested on a PC with a 3.60 GHz i7-4790 CPU and 16 GB RAM. In this section, some examples are presented, comparison with classical methods and some implementation details are discussed.

4.1. Solution to complex models with non-zero genus

Because the genus of a trivariate B-spline solid is zero, it cannot fit a 3D model with non-zero genus directly. Generally, when a 3D model with non-zero genus is required to be fitted using a trivariate B-spline solid, it is segmented into sub-parts with zero genus. Then, each sub-part is fitted using a single trivariate B-spline solid, and all of the B-spline solids are stitched into a unified solid, forming the trivariate solid fitting the original 3D model with non-zero genus. It is the widely employed strategy for fitting 3D model with non-zero genus and lots of methods have been developed to handle the continuity problems in stitching adjacent B-spline patches and solids [31].

As illustrated in Fig. 7, the given mesh model *Eight* (Fig. 7(a)) with non-zero genus is first segmented into six sub-parts (Fig. 7(b)), and each sub-part is fitted by a trivariate B-spline solid (Fig. 7(c)). Next, the TDF is designed in the parametric domain of each B-spline solid. In our implementation, adjacent trivariate B-spline solids, as well as the TDFs therein, are made C^1 continuous. Finally, by mapping the volume TPMS structures in the parametric domains into the B-spline solids, the heterogeneous porous scaffold in the mesh model *Eight* is generated (Fig. 7(d)).

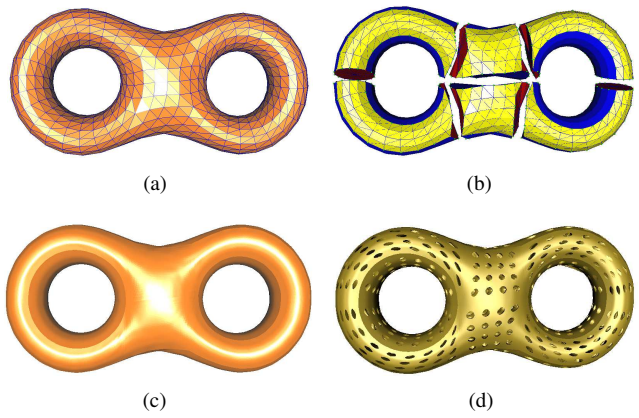

Figure 7. Heterogeneous porous scaffold in the model *Eight* with non-zero genus. (a) Mesh model *Eight* with non-zero genus. (b) Segmented sub-parts. (c) Stitched trivariate B-spline solid. (d) P-type pore structure scaffold.

4.2. Comparison with classical methods

The heterogeneous porous scaffold generation method developed in this study is compared with three classical methods presented in Refs. [4, 6, 8], respectively. The method developed in [4] produces a porous scaffold by first immersing a hexahedral mesh model in an ambient TPMS structure, and then taking the intersection of them as the porous scaffold. Therefore, this method cannot guarantee the completeness of the boundary TPMS units. As shown in Fig. 8(a), many boundary TPMS units are broken.

In the method proposed in [6], a fourth coordinate is firstly added into each control point of a T-spline solid, which determines the threshold field, and then an ambient TPMS. Secondly, the T-spline solid is discretized into a hexahedral mesh. Finally, the porous scaffold is generated by intersecting the hexahedral mesh with the ambient TPMS. Then, the porous scaffold generated by the method in [6] still contains broken boundary TPMS units, as illustrated in Fig. 8(b).

Finally, in the method presented in [8], the porous scaffold is generated by mapping a regular TPMS unit into the hexahedrons of a parameterized hexahedral mesh with a trilinear interpolation. However, because the mappings from the TPMS unit to the hexahedrons are performed one by one independently, the continuity between adjacent TPMS units in adjacent hexahedrons cannot be guaranteed. For example, in Fig. 8(c), the triangular meshes of two adjacent TPMS units are mismatched. Moreover, because the threshold value C of all TPMS units is a constant, the porosity is difficult to adjust in the method [8].

However, because our method generates a heterogeneous porous scaffold by mapping a unitary TPMS in the parametric domain to a trivariate B-spline solid, it avoids the shortcomings of the aforementioned three methods. The heterogeneous porous scaffold generated by our method has the following properties (Fig. 8(d)):

- Completeness of TPMS units and continuity between adjacent TPMS units are guaranteed.
- The TDF can be easily designed.
- The TDF file format saves significant storage space.

4.3. Manufacturing results and mechanical performance

As stated above, while hexahedral meshes are employed in the two methods developed in [4] and [8], our method and the method developed in [6] both use trivariate parametric solids, i.e., T-spline solid in [6], and B-spline solid in our method. Moreover, our method and the method [6] can both control the porosity distribution by trivariate parametric functions. Therefore, the heterogeneous porous scaffolds designed using our method (abbreviated as TDF based porous scaffold) and the method in [6] (abbreviated as T-spline porous scaffold) are manufactured using a 3D printer (SLA: stereo lithography apparatus) to compare their mechanical performances (Fig. 9). The material is special photosensitive resin, and the printing thickness is set as $0.1mm$. The porosity distributions of the two porous scaffolds are made the same by setting the same trivariate parametric function, and the printing sizes are both set as $87mm \times 100mm \times 89mm$ (Fig. 9). In addition, as shown in Fig. 9, the weights of the two porous scaffolds are $86.073g$ (T-spline porous scaffold) and $80.834g$ (TDF based porous scaffold), respectively. The printed T-spline porous scaffold is 6.48% heavier than the TDF based porous scaffold.

Moreover, we use an electromechanical universal testing machine to physically evaluate the strength of the printed models under mechanical pressure from the same direction (Fig. 10(a)), and plot the load-displacement curves in Fig. 10(b), where the orange and blue curves are the mechanical test results of the TDF based porous scaffold and T-spline porous scaffold, respectively. As shown in Fig. 10(b), while the T-spline porous

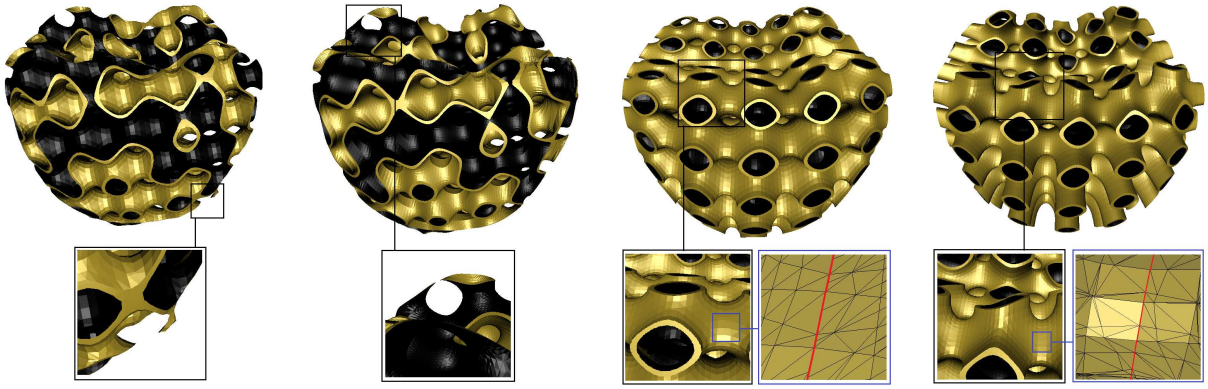

(a) Method in [4]. (b) Method in [6]. (c) Method in [8]. (d) Our method.

Figure 8. Comparison with classical porous scaffold generating methods. The methods in [4] (a) and [6] (b) cannot guarantee the completeness, and there are broken boundary units in the generated porous scaffold (a, b). The method in [8] (c) cannot ensure the continuity between adjacent TPMS units, and the triangular meshes of the two adjacent TPMS units in the porous scaffold are mismatched along the red boundary curve (c). On the contrary, the porous scaffold generated by our method is completed and continuous (d).

Table 2. Statistical data of the heterogeneous porous scaffold generation method developed in this paper.

Model	Type	Structure	Period coefficients	Run time(s)[1]			Storage space(MB)[2]	
				TDF	TPMS	Porous scaffold	STL format	TDF format
Ball joint	P	pore	(16, 14, 18)	2.745	0.326	1.466	722.428	0.813
		rod			0.319	1.421	704.105	
		sheet			0.658	2.836	1355.363	
Venus	D	pore	(10, 10, 10)	2.728	0.293	1.394	701.682	0.947
		rod			0.286	1.383	695.595	
		sheet			0.528	2.699	1359.087	
Tooth	G	pore	(8, 6, 8)	2.732	0.238	0.926	407.188	0.538
		rod			0.237	0.931	407.202	
		sheet			0.499	1.789	789.972	
Moai	I-WP	pore	(6, 6, 16)	2.736	0.290	1.286	621.676	0.829
		rod			0.284	1.301	614.045	
		sheet			0.583	2.537	1212.565	

[1] Run time (in second) for TDF construction, generation of volume TPMS and heterogeneous porous scaffold.
[2] Storage space (in megabyte) of heterogeneous porous scaffolds using the traditional STL file format and the TDF file format.

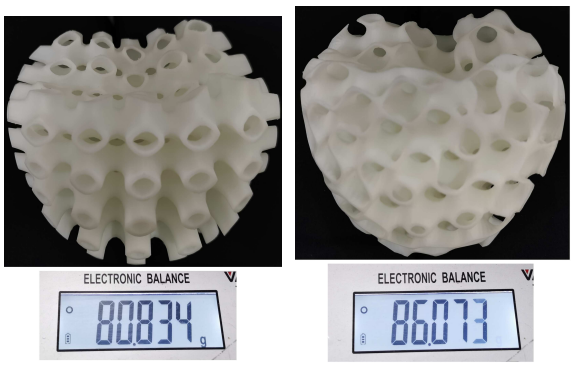

(a) (b)

Figure 9. Two 3D printed (SLA) porous scaffolds and their weights. (a) TDF based porous scaffold. (b) T-spline porous scaffold.

scaffold can sustain just about 2050N external force, our TDF based porous scaffold can sustain external force 3080N or so. Moreover, in Fig. 10(b), while the orange curve decreases at about 3080N external force, the first decreasing of the blue curve appears at about 1140N external force. The decreasing of the load-displacement curve means that fracture occurs. Therefore, the T-spline porous scaffold begins to fracture at an external force (1140N), much less than that of the TDF based porous scaffold (3080N). Finally, with the same external force being applied to the porous scaffolds (refer to Fig. 10(b)), the T-spline porous scaffold (blue curve) displaces larger than TDF based porous scaffold (orange curve), meaning that the TDF based porous scaffold performs better than the T-spline porous scaffold in strength.

In the mechanical test, it was noticed that the T-spline porous scaffold begins to fracture at the places where the TPMS units are incomplete. Therefore, we think that the completeness is an important factor for the strength of a porous scaffold. Because the TPMS units of the TDF based porous scaffold are all complete, and some TPMS units of the T-spline porous scaffold are not complete, the TDF based porous scaffolds perform better than the T-spline porous scaffolds in terms of strength.

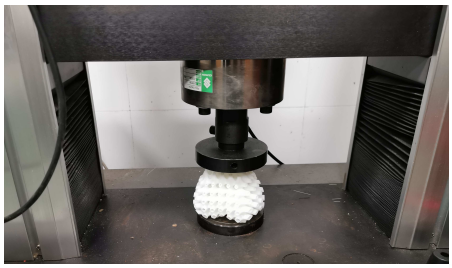

(a)

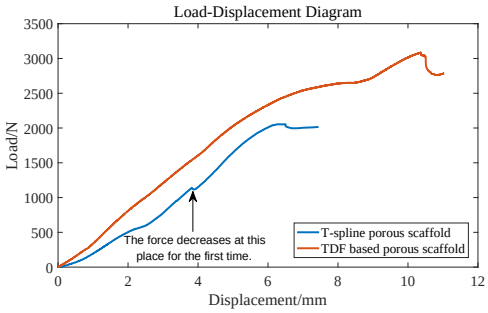

(b)

Figure 10. Mechanical test and the load-displacement curve. (a) Mechanical test using an electromechanical universal testing machine. (b) The load-displacement curves for TDF based porous scaffold (in orange) and T-spline porous scaffold (in blue).

4.4. Experimental examples

In this section, some heterogeneous porous scaffold results generated by our method are presented (Figs. 11-14). In Figs. 11-14, (a) is the input trivariate B-spline solid, (b) is the TDF designed by the above methods, and (c,d, and e) are the heterogeneous porous scaffolds of pore structure, rod structure, and sheet structure with different TPMS types, all generated based on (b).

Specially, the TDFs in Figs. 11 and 12 are designed using the physical domain based method, where the mean curvatures on the boundary surface of a trivariate B-spline solid are diffused inside. In Fig. 13 and 14, the heterogeneous porous scaffolds are generated by the porosity preservation method. In Fig. 13, the porosities at the physical grid vertices are set as 0.5. In Fig. 14, the porosity Por_i at the physical grid vertex (x_i, y_i, z_i) is specified as,

$$Por_i = 0.3\left(1 - \frac{z_i - z_{min}}{z_{max} - z_{min}}\right) + 0.7\frac{z_i - z_{min}}{z_{max} - z_{min}},$$

where $z_{min} = min_i\{z_i\}$, and $z_{max} = max_i\{z_i\}$.

Moreover, statistical data are listed in Table 2, including period coefficients (ρ_u, ρ_v, ρ_w), run times for the TDF construction, porosity preservation, TPMS triangulation, and heterogeneous porous scaffold generation, and storage costs of porous scaffolds with the traditional STL file format and the new TDF file format.

4.5. TDF file format

In Table 2, the storage spaces required to store the porous scaffolds using the traditional STL file format and the new TDF file format are listed. Storing the porous scaffolds using the TDF file format costs 0.538 to 0.947 MB, while using the STL file format, it costs 407.188 to 1359.087 MB. Therefore, at least 99% of storage space is saved by using the new TDF file format. Moreover, in Table 2, the time cost for generating the heterogeneous porous scaffold from the TDF file format is also listed, including the run time for generating volume TPMS structures and porous scaffolds. We can see that the time costs range from 4 to 7 seconds, which is acceptable for user interaction.

The TDF file format brings some extra benefits. Traditionally, heterogeneous porous scaffolds have been stored as linear mesh models. However, the TDF file format stores a trivariate B-spline function. Therefore, in theory, a porous scaffold can be generated to any prescribed precision using the TDF file format. In addition, the period coefficients and control points of the trivariate B-spline function, stored in the TDF file format, can be taken as some types of *parameters*. Therefore, a heterogeneous porous scaffold can be changed by altering these parameters, just like the parametric modeling technique.

4.6. Discussion

In this section, we will discuss the advantages and limitations of the developed method (abbr. TDF based method), which are untouched in the above.

On the one hand, the TDF based method has some extra advantages. First, the heterogeneous porous scaffold generated by the TDF based method is fully determined by the TPMS in the parametric domain. Because the parametric domain is a cubic domain, the other types of porous structures, such as those developed in [32, 33], are easily produced in the cubic parameter domain. Therefore, the TDF based method can be extended to generate the other types of porous structures.

On the other hand, the limitations of the TDF based method are evident. First of all, because a trivariate B-spline solid has zero genus, a single B-spline solid cannot represent the 3D model with non-zero genus. As stated in Section 4.1, to represent a 3D model with non-zero genus using B-spline solids, it should be segmented into sub-parts with zero-genus. The segmentation of the 3D model is tedious, usually needing user interaction.

Moreover, though the TDF file format can save considerable storage space, it is still required to convert to the traditional file formats for manufacturing. Therefore, as the future work, we will study how to manufacture the models stored in TDF file format directly, avoiding the conversion to the traditional file formats.

5. Conclusion

In this study, we developed a method for generating a heterogeneous porous scaffold in a trivariate B-spline solid by the TDF designed in the parametric domain. First, the TDF is easy to be designed in the cubic parametric domain, and is

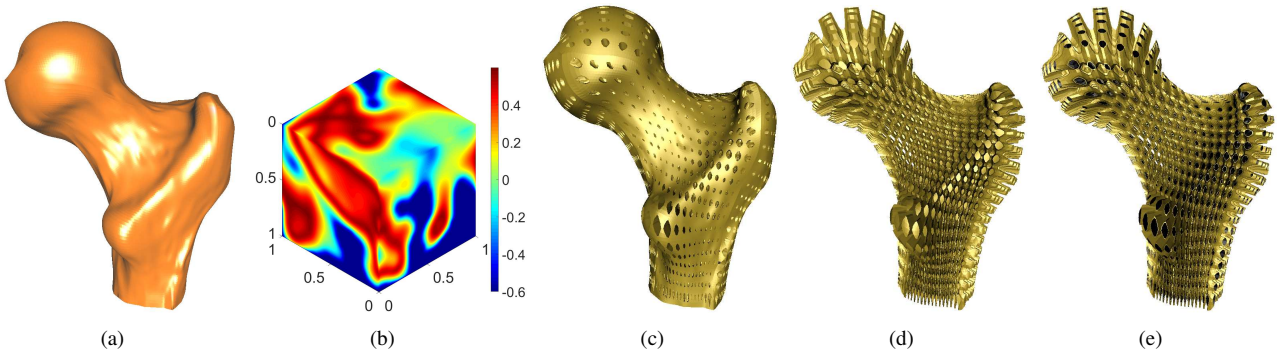

Figure 11. Heterogeneous porous scaffold of *Ball-joint*. (a) Trivariate B-spline solid. (b) TDF designed by the physical domain based method with mean curvatures. (c) P-type pore structure. (d) P-type rod structure. (e) P-type sheet structure.

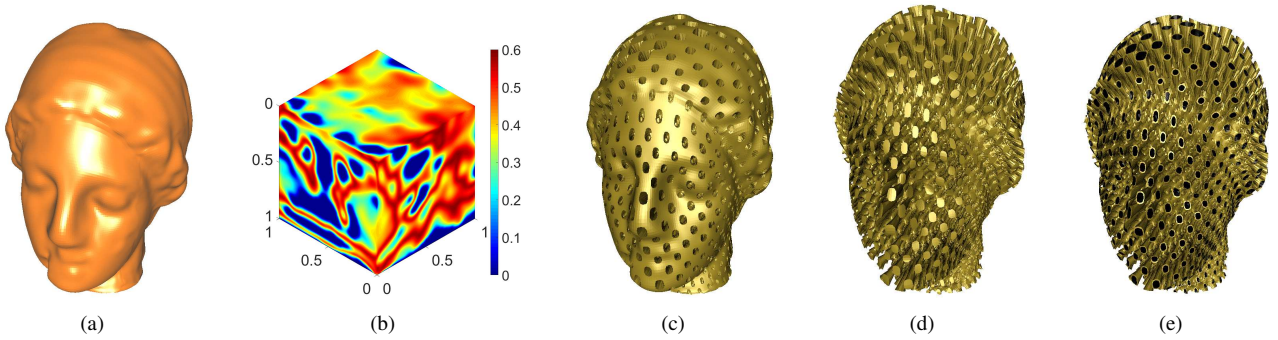

Figure 12. Heterogeneous porous scaffold of *Venus*. (a) Trivariate B-spline solid. (b) TDF designed by the physical domain based method with mean curvatures. (c) D-type pore structure. (d) D-type rod structure. (e) D-type sheet structure.

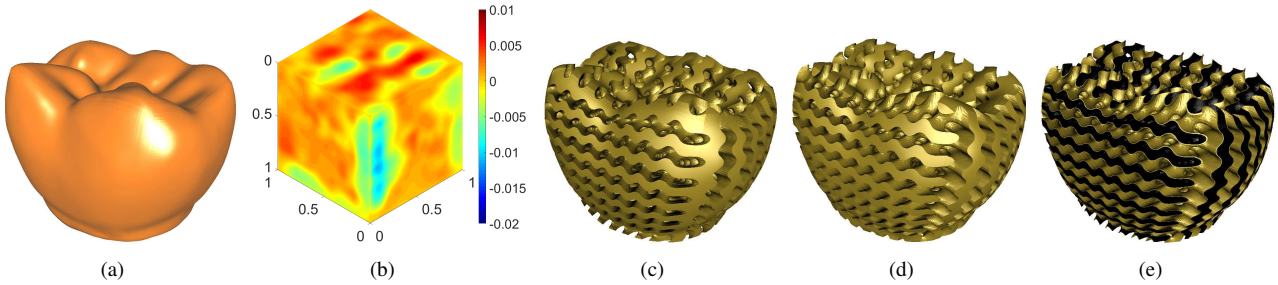

Figure 13. Heterogeneous porous scaffold of *Tooth*. (a) Trivariate B-spline solid. (b) TDF generated after porosity preservation. (c) G-type pore structure. (d) G-type rod structure. (e) G-type sheet structure.

represented as a trivariate B-spline function, which can be employed to control some physical properties, such as porosity, of the porous scaffold. Then, a TPMS can be generated in the parametric domain based on the TDF. Finally, by mapping the TPMS into the B-spline solid, a heterogeneous porous scaffold is produced. Moreover, we presented a new file format (TDF) for storing the porous scaffold, that saves significant storage space. By the method developed in this study, both completeness of the TPMS units and continuity between adjacent TPMS units can be guaranteed. More importantly, the TDF file format not only saves significant storage space, but it can also be used to generate a porous scaffold to any prescribed precision. In terms of future work, determining how to change the shape of a porous scaffold using the parameters stored in the TDF file format is a promising research direction.

References

[1] A. Yánez, A. Cuadrado, O. Martel, H. Afonso, D. Monopoli, Gyroid porous titanium structures: a versatile solution to be used as scaffolds in bone defect reconstruction, Materials & Design 140 (2018) 21–29. 1

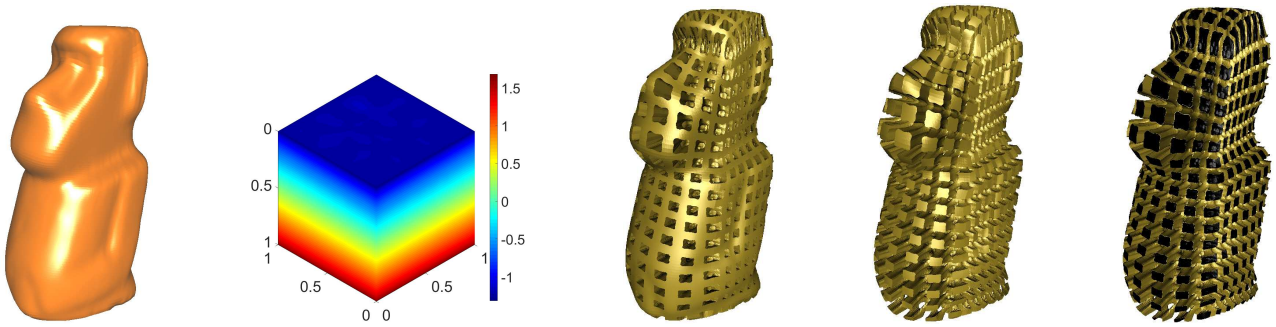

(a) (b) (c) (d) (e)

Figure 14. Heterogeneous porous scaffold of *Moai*. (a) Trivariate B-spline solid. (b) TDF generated after porosity preservation. (c) I-WP-type pore structure. (d) I-WP-type rod structure. (e) I-WP-type sheet structure.

[2] H. G. V. Schnering, R. Nesper, Nodal surfaces of Fourier series: fundamental invariants of structured matter, Zeitschrift Für Physik B Condensed Matter 83 (3) (1991) 407–412. 1, 3

[3] D. Yoo, Porous scaffold design using the distance field and triply periodic minimal surface models, Biomaterials 32 (31) (2011) 7741–7754. 1, 2

[4] D. Yoo, Heterogeneous minimal surface porous scaffold design using the distance field and radial basis functions, Medical Engineering & Physics 34 (5) (2012) 625–639. 1, 2, 8, 9

[5] N. Yang, K. Zhou, Effective method for multi-scale gradient porous scaffold design and fabrication, Materials Science & Engineering: C 43 (2014) 502–505. 1, 2

[6] J. Feng, J. Fu, C. Shang, Z. Lin, B. Li, Porous scaffold design by solid T-splines and triply periodic minimal surfaces, Computer Methods in Applied Mechanics & Engineering 336 (2018) 333–352. 1, 2, 3, 8, 9

[7] D. Yoo, Computer-aided porous scaffold design for tissue engineering using triply periodic minimal surfaces, International Journal of Precision Engineering & Manufacturing 12 (1) (2011) 61–71. 1

[8] H. Chen, Y. Guo, R. Rostami, S. Fan, K. Tang, Z. Yu, Porous structure design using parameterized hexahedral meshes and triply periodic minimal surfaces, in: Computer Graphics International 2018, ACM Press, 2018, pp. 117–128. 1, 2, 8, 9

[9] J. Shi, L. Zhu, L. Li, Z. Li, J. Yang, X. Wang, A TPMS-based method for modeling porous scaffolds for bionic bone tissue engineering, Scientific Reports 8 (1) (2018) 7395. 1, 2

[10] S. Vijayavenkataraman, L. Zhang, S. Zhang, J. Y. Hsi Fuh, W. F. Lu, Triply periodic minimal surfaces sheet scaffolds for tissue engineering applications: an optimization approach toward biomimetic scaffold design, ACS Applied Bio Materials 1 (2) (2018) 259–269. 1

[11] H.-J. Sung, C. Meredith, C. Johnson, Z. S. Galis, The effect of scaffold degradation rate on three-dimensional cell growth and angiogenesis, Biomaterials 25 (26) (2004) 5735–5742. 1

[12] H. G. Lee, J. Park, S. Yoon, C. Lee, J. Kim, Mathematical model and numerical simulation for tissue growth on bioscaffolds, Applied Sciences 9 (19) (2019) 4058. 1

[13] S. Rajagopalan, R. A. Robb, Schwarz meets Schwann: design and fabrication of biomorphic tissue engineering scaffolds, Medical Image Analysis 10 (5) (2006) 693–712. 2

[14] F. P. Melchels, K. Bertoldi, R. Gabbrielli, A. H. Velders, J. Feijen, D. W. Grijpma, Mathematically defined tissue engineering scaffold architectures prepared by stereolithography, Biomaterials 31 (27) (2010) 6909–6916. 2

[15] B. Li, J. Fu, Y. J. Zhang, W. Lin, C. Shang, Slicing heterogeneous solid using octree-based subdivision and trivariate T-splines for additive manufacturing, Rapid Prototyping Journal ahead-of-print. 2

[16] B. Li, J. Fu, Y. J. Zhang, A. Pawar, A trivariate T-spline based framework for modeling heterogeneous solids, Computer Aided Geometric Design 81 (2020) 101882. 2

[17] T. J. R. Hughes, J. A. Cottrell, Y. Bazilevs, Isogeometric analysis: CAD, finite elements, NURBS, exact geometry and mesh refinement, Computer Methods in Applied Mechanics & Engineering 194 (39) (2005) 4135–4195. 2

[18] Y. Zhang, Y. Bazilevs, S. Goswami, C. L. Bajaj, T. J. Hughes, Patient-specific vascular NURBS modeling for isogeometric analysis of blood flow, Computer Methods in Applied Mechanics & Engineering 196 (29) (2007) 2943–2959. 2

[19] T. Martin, E. Cohen, R. M. Kirby, Volumetric parameterization and trivariate B-spline fitting using harmonic functions, Computer Aided Geometric Design 26 (6) (2009) 648–664. 2

[20] M. Aigner, C. Heinrich, B. Jüttler, E. Pilgerstorfer, B. Simeon, A. V. Vuong, Swept volume parameterization for isogeometric analysis, in: Mathematics of Surfaces XIII, Springer Berlin Heidelberg, Berlin, Heidelberg, 2009, pp. 19–44. 2

[21] G. Xu, B. Mourrain, R. Duvigneau, A. Galligo, Analysis-suitable volume parameterization of multi-block computational domain in isogeometric applications, Computer-Aided Design 45 (2) (2013) 395–404. 2

[22] X. Wang, X. Qian, An optimization approach for constructing trivariate B-spline solids, Computer-Aided Design 46 (1) (2014) 179–191. 2

[23] H. Lin, S. Jin, Q. Hu, Z. Liu, Constructing B-spline solids from tetrahedral meshes for isogeometric analysis, Computer Aided Geometric Design 35-36 (2015) 109–120. 2

[24] A. Piegl, Les, W. Tiller, The NURBS Book, Springer Berlin Heidelberg, Berlin, Heidelberg, 1997. 2

[25] P. J. F. Gandy, S. Bardhan, A. L. Mackay, J. Klinowski, Nodal surface approximations to the P, G, D and I-WP triply periodic minimal surfaces, Chemical Physics Letters 336 (3) (2001) 187–195. 3

[26] W. Yan, Periodic surface modeling for computer aided nano design, Computer-Aided Design 39 (3) (2007) 179–189. 3

[27] A. Doi, A. Koide, An efficient method of triangulating equivalued surfaces by using tetrahedral cells, Ieice Trans 74 (1) (1991) 214–224. 3

[28] D. A. Field, Laplacian smoothing and Delaunay triangulations, Communications in Applied Numerical Methods 4 (6) (1988) 709–712. 4

[29] C. Deng, H. Lin, Progressive and iterative approximation for least squares B-spline curve and surface fitting, Computer-Aided Design 47 (1) (2014) 32–44. 4, 5

[30] M. T. Heath, Scientific Computing: An Introductory Survey, Revised Second Edition, Society for Industrial and Applied Mathematics, 2018. 6, 7

[31] H. Lin, H. Huang, C. Hu, Trivariate B-spline solid construction by pillow operation and geometric iterative fitting, SCIENCE CHINA (Information Sciences) 61 (2018) 232–234. 8

[32] S. Cai, J. Xi, A control approach for pore size distribution in the bone scaffold based on the hexahedral mesh refinement, Computer-Aided Design 40 (10-11) (2008) 1040–1050. 10

[33] X. Kou, S. Tan, A simple and effective geometric representation for irregular porous structure modeling, Computer-Aided Design 42 (10) (2010) 930–941. 10

Appendix A: TDF file format

#TPMS type
m=0 : P-type; m=1 : G-type; m=2 : D-type; m=3 : I-WP-type;
m
#structure type
n=0 : Rod structure; n=1 : Pore structure; n=2 : Sheet structure;
n
#period coefficients(ρ_u, ρ_v, ρ_w)
$\rho_u\ \rho_v\ \rho_w$
#resolution of control grid of TDF
$n_u + 1\ n_v + 1\ n_w + 1$
#control points of TDF
$C_{0,0,0}$
$C_{0,0,1}$
$\vdots$
C_{n_u,n_v,n_w}
#knot vector in u-direction of TDF
$u_0\ u_1 \cdots u_{n_u+4}$
#knot vector in v-direction of TDF
$v_0\ v_1 \cdots v_{n_v+4}$
#knot vector in w-direction of TDF
$w_0\ w_1 \cdots w_{n_w+4}$
#resolution of control grid of trivariate B-spline solid
$m + 1\ n + 1\ l + 1$
#control points of trivariate B-spline solid
$x_{0,0,0}\ y_{0,0,0}\ z_{0,0,0}$
$x_{0,0,1}\ y_{0,0,1}\ z_{0,0,1}$
$\vdots \quad \vdots \quad \vdots$
$x_{m,n,l}\ y_{m,n,l}\ z_{m,n,l}$
#knot vector in u-direction of trivariate B-spline solid
$U_0\ U_1 \cdots U_{m+4}$
#knot vector in v-direction of trivariate B-spline solid
$V_0\ V_1 \cdots V_{n+4}$
#knot vector in w-direction of trivariate B-spline solid
$W_0\ W_1 \cdots W_{l+4}$

Appendix B: Functions between the porosity and the threshold C

In order to ensure the fitting error reaches 10^{-5}, we use linear or quadratic functions to fit the relationship between the porosity and the threshold C.

Pore structures shown in Fig. 4(a)
P-type: $Por = 0.2887C + 0.5001,\ C \in [-0.8, 0.8]$,
D-type: $Por = 0.5898C + 0.5001,\ C \in [-0.6, 0.6]$,
G-type: $Por = 0.3338C + 0.4998,\ C \in [-0.8, 0.8]$,
I-WP-type: $Por = -0.1332C + 0.5243,\ C \in [-2.0, 2.0]$.

Rod structures shown in Fig. 4(b)
P-type: $Por = -0.2887C + 0.4999,\ C \in [-0.8, 0.8]$,
D-type: $Por = -0.5898C + 0.4999,\ C \in [-0.6, 0.6]$,
G-type: $Por = -0.3338C + 0.5002,\ C \in [-0.8, 0.8]$,
I-WP-type: $Por = 0.1332C + 0.4757,\ C \in [-2.0, 2.0]$.

Sheet structures shown in Fig. 4(c)
P-type: $Por = -0.0009C^2 + 0.00005C + 0.943,\ C \in [-0.6, 0.8]$,
D-type: $Por = -0.0.0151C^2 + 0.003C + 0.8839,\ C \in [-0.4, 0.6]$,
G-type: $Por = -0.0048C^2 + 0.0001C + 0.9357,\ C \in [-0.6, 0.8]$,
I-WP-type: $Por = -0.0006C^2 - 0.0021C + 0.974,\ C \in [-1.8, 2.0]$.